East European Journal of Physics. 1. 343-350 (2026)
DOI:10.26565/2312-4334-2026-1-40 ISSN 2312-4334

CRYOGENIC MATERIAL AND ELECTROPHYSICAL CHANGES IN Si AND GaAs

Jonibek Sh. Abdullayev[1]*, Madinabonu Sh. Ibragimova[1], Jo'shqin Sh. Abdullayev[2], Ibrokhim B. Sapaev[2,3,4,5]

[1]*Urgench State University, Hamid Olimjon Street, 14, Urgench, 220100 Uzbekistan*
[2]*National Research University TIIAME, Department of Physics and Chemistry, Tashkent, Uzbekistan*
[3]*Western Caspian University, Baku, Azerbaijan*
[4]*Scientific Researcher, Tashkent University for Applied Sciences, 28 Universitetskaya Street, Tashkent 100095, Uzbekistan*
[5]*School of Engineering, Central Asian University, Tashkent 111221, Uzbekistan*
**Corresponding Author e-mail: j.sh.abdullayev6@gmail.com*
Received October 5, 2025; revised January 31, 2026; accepted February 3, 2026

This study presents a comprehensive investigation of the cryogenic electrical and material behavior of silicon (Si) and gallium arsenide (GaAs) over a wide temperature range from 4 to 300 K and doping concentrations spanning intrinsic conditions up to 1×10^{18} cm^{-3}. The temperature-dependent evolution of both the fundamental and effective band gap energies is systematically quantified, revealing a band gap widening from 1.12 to 1.17 eV in Si and from 1.42 to 1.51 eV in GaAs as the temperature is reduced from room temperature to 4 K. Detailed analysis of donor and acceptor activation energies demonstrates pronounced incomplete ionization at cryogenic temperatures, particularly below 20 K, where the free carrier concentration in lightly doped samples decreases by nearly 80%, resulting in a substantial suppression of electrical conductivity. In addition, surface-sensitive chemical characterization confirms strongly reduced dopant diffusion and negligible oxidation at low temperatures, indicating excellent structural and chemical stability in both materials. The combined electrical and surface analyses elucidate the intricate interplay between band structure evolution, carrier freeze-out dynamics, and surface processes under cryogenic conditions. These findings provide critical physical insight and practical design guidelines for the development of high-performance cryogenic electronic, optoelectronic, and quantum-enabled devices based on Si and GaAs platforms.
Keywords: *Effective band gap; Electrostatic potential; Incomplete ionization; Carrier concentration; Band gap widening; Low-temperature effects; Cryogenic semiconductors; Electrical conductivity*
PACS: 73.40. Lq, 73.61.Cw, 73.61.Ey, 72.20.Jv

INTRODUCTION

The ongoing progress in semiconductor technology relies heavily on a deep comprehension of the fundamental physical, chemical, and mathematical principles that dictate device behavior. Central to modern electronics and optoelectronics is the p–n junction, which serves as the core building block for a variety of devices, including solar cells, light-emitting diodes (LEDs), photodetectors, and nanowire-based systems [1–3]. Silicon (Si) has long been the dominant material in the industry due to its natural abundance, mature and reliable fabrication techniques, and favorable electronic properties [4–6]. Conversely, gallium arsenide (GaAs), characterized by high electron mobility and a direct bandgap energy, is particularly advantageous for high-speed electronic circuits and cutting-edge optoelectronic devices [7–9].

In recent years, non-planar junction designs have garnered significant interest. Radial p–n junctions (RHJs) offer distinct advantages over planar counterparts, including increased effective surface area, enhanced optical absorption, superior light-trapping efficiency, and geometry-induced modifications to the local electrostatic field [10–13]. These characteristics make RHJs highly promising for nanoscale devices, cryogenic electronics, and high-efficiency optoelectronic systems [14–16].

The electrostatics of semiconductor junctions is governed by Poisson's equation, which establishes a self-consistent relationship between charge density and electrostatic potential [17–19]. While Cartesian coordinates suffice for planar junctions, cylindrical coordinates are essential for accurately describing radial junctions, where curvature effects significantly influence the local electric field [23–25]. These geometric differences directly affect depletion widths, junction capacitance, and overall device performance. At cryogenic temperatures, incomplete ionization of dopants introduces additional complexity, as a substantial fraction of donors and acceptors remain neutral [26–29]. This deviation from the full-ionization assumption necessitates probabilistic modeling based on Fermi–Dirac statistics and dopant activation energies [30–33], leading to temperature-dependent modifications of space-charge density, electrostatic potential, and capacitance–voltage (C–V) characteristics [34–36,43].

Beyond conventional Si and GaAs systems, diluted magnetic semiconductors (DMS), such as GaMnAs cylindrical nanoshells, display rich thermodynamic and magnetic behavior influenced by Rashba spin–orbit (RSO) coupling arising from structural inversion asymmetry [39–40]. Numerical analyses combining Schrödinger equation solutions with Boltzmann-Gibbs statistics reveal competing effects: external magnetic fields enhance orbital confinement, whereas RSO coupling delocalizes electron wavefunctions. This interplay governs key thermodynamic quantities, including heat

Cite as: J.Sh. Abdullayev, M.Sh. Ibragimova, J.Sh. Abdullayev, I.B. Sapaev, East Eur. J. Phys. 1, 343 (2026), https://doi.org/10.26565/2312-4334-2026-1-40

capacity—exhibiting low-temperature Schottky anomalies—and magnetic susceptibility, which strongly depends on both temperature and field. Additionally, these systems undergo temperature- and field-driven ferromagnetic-to-paramagnetic phase transitions, underscoring their potential for spintronic applications.

A systematic comparative study of planar and radial p–n junctions under incomplete ionization conditions is thus crucial. Cylindrical-coordinate formulations for radial geometries capture curvature-enhanced electric fields and extended depletion regions. In this work, we develop a comprehensive mathematical framework for analyzing electrostatic potential profiles, depletion widths, and electric-field distributions in Si- and GaAs-based planar and radial junctions at cryogenic temperatures, offering both theoretical insights and practical guidance for the design of advanced nanoscale optoelectronic and spintronic devices.

METHODS AND MATERIAL

In semiconductor physics, one of the most critical parameters is the energy band gap, which defines the energy difference between the valence and conduction bands. Traditionally, most literature reports and device models consider only the fundamental band gap energy, corresponding to intrinsic (undoped) materials even p-tye and n-type exist [35,26,16]. However, when donor or acceptor impurities are introduced into the crystal lattice, the band structure is modified due to impurity-induced states, leading to the formation of an effective band gap rather than the ideal fundamental one. In this case, the effective band gap represents the actual energy separation between occupied and unoccupied electronic states in extrinsic semiconductors, and it deviates from the intrinsic value depending on the doping level and temperature. This distinction becomes especially important at low temperatures, where incomplete ionization of dopants occurs, causing significant deviations in carrier concentration and band-edge positions.

In conventional models, the fundamental band gap is often assumed to be temperature dependent but unaffected by dopant ionization. However, in reality, only the effective band gap changes noticeably under varying doping and temperature conditions, particularly in cryogenic regimes. Considering these effects, silicon (Si) is investigated here as a technologically dominant material in microelectronics, while gallium arsenide (GaAs) is selected for its superior optoelectronic performance. The functional parameters of these two materials used in the present analysis are summarized in Table 1.

Table 1. Fundamental physical, electrical, and optical parameters of Silicon (Si) and Gallium Arsenide (GaAs) at 300 K [40-43].

Parameter	**Symbol**	**Si (Silicon)**	**GaAs (Gallium Arsenide)**	**Units / Notes**
Crystal structure	—	Diamond cubic	Zinc blende	—
Lattice constant	a_o	5.431	5.653	Å
Density	P	2.33	5.32	g/cm³
Atomic weight	—	28.09	144.64	—
Relative permittivity (static)	ε_r	11.7	12.9	—
Band gap (300 K)	Eg	1.12 (indirect)	1.42 (direct)	eV
Band gap at 0 K	Eg(0)	1.17	1.519	eV
Varshni parameter α	α	4.73×10^{-4}	5.41×10^{-4}	eV/K
Varshni parameter β	β	636	204	K
Electron affinity	χ	4.05	4.07	eV
Conduction band effective DOS	Nc	2.8×10^{19}	4.7×10^{17}	cm^{-3}
Valence band effective DOS	Nv	1.04×10^{19}	7.0×10^{18}	cm^{-3}
Intrinsic carrier concentration	n_i	1.5×10^{10}	2.1×10^{6}	cm^{-3}
Electron effective mass	m_h^*	0.26 m_0 (trans.)	0.067 m_0	—
Hole effective mass	m_e^*	0.55 m_0	0.5 m_0	—
Electron mobility	μ_n	1350	8500	$cm^2/V\cdot s$
Hole mobility	μ_p	480	400	$cm^2/V\cdot s$
Electron diffusion coefficient	D_n	35	220	cm^2/s
Hole diffusion coefficient	D_p	12	10	cm^2/s
Saturation velocity	v_{sat}	1×10^{7}	2×10^{7}	cm/s
Thermal conductivity	κ	1.5	0.46	W/cm·K
Thermal expansion coefficient	α_T	2.6×10^{-6}	5.7×10^{-6}	K^{-1}
Melting point	T_m	1414	1238	K
Specific heat capacity	C_p	0.70	0.35	J/g·K
Refractive index (λ = 1 μm)	n	3.48	3.3	—
Energy gap type	—	Indirect (Γ–X)	Direct (Γ–Γ)	—

The fundamental (intrinsic) bandgap energy, $E_g(T)$ is the energy difference between the conduction band minimum and valence band maximum, for an ideal pure crystal. However, in doped or real semiconductors, several effects modify

the bandgap energy, producing an effective bandgap energy $E_{g,eff}(T)$ that depends on: Temperature (T), Doping concentration (N_D, N_A), Bandgap energy narrowing (BGN), Carrier–carrier and impurity interactions. Temperature dependence – Varshni's equation (1) [17].

$$E_g(T) = E_g(0) - \frac{\alpha T^2}{T+\beta} \tag{1}$$

Where $E_g(0)$ is the bandgap energy at 0 K. The empirical parameters used were $\alpha = 4.73\times10^{-4}$ eV/K and $\beta = 636$ K for Si, and $\alpha = 5.405\times10^{-4}$ eV/K and $\beta = 204$ K for GaAs. Bandgap energy narrowing (due to heavy doping): When doping is high ($\geq10^{18}$ cm^{-3}), impurity band formation and many-body effects cause a reduction in bandgap energy [25]:

$$E_{g,eff}(T) = E_g(T) - \Delta E_{BGN} \tag{2}$$

where ΔE_{BGN} bandgap energy narrowing term $E_g(T)$. Effective bandgap energy accounts for temperature- and doping-induced narrowing of the ideal bandgap energy. It's crucial for modeling carrier concentration, recombination, and device characteristics in real semiconductors.

RESULTS AND DISCUSSION

At cryogenic temperature (T ≈ 1 K), the fundamental bandgap energy $E_g(T)$ of Si is 1.17 eV, while that of GaAs is 1.519 eV, consistent with experimental low-temperature data. As the temperature rises, both materials show a monotonic decrease in $E_g(T)$ as a result of thermal lattice expansion and enhanced electron–phonon coupling. At room temperature (300 K), $E_g(T)$ decreases to approximately 1.12 eV for Si and 1.42 eV for GaAs, representing reductions of ≈ 4.3 % and ≈ 6.5 %, respectively. The stronger temperature sensitivity in GaAs originates from its higher Varshni coefficient ($\alpha = 5.405\times10^{-4}$ eV/K) and smaller temperature parameter ($\beta = 204$ K) compared to Si ($\alpha = 4.73\times10^{-4}$ eV/K, $\beta = 636$ K). When the doping concentration increases from 1×10^{17} to 1×10^{18} cm^{-3}[17], the effective bandgap energy $E_{g,eff}(T)$ decreases further owing to BGN effects induced by impurity potential fluctuations, carrier–carrier interactions, and band-tail formation. At 300 K, the calculated narrowing is approximately 0.030–0.045 eV for Si and 0.020–0.035 eV for GaAs, resulting in $E_{g,eff}(T) = 1.08-1.09\ eV$ for Si and 1.38–1.40 eVfor GaAs. This indicates that Si experiences a stronger BGN effect (≈ 35–45 meV) than GaAs (≈ 25–30 meV), attributed to its indirect band structure and higher density of electronic states near the band edges.

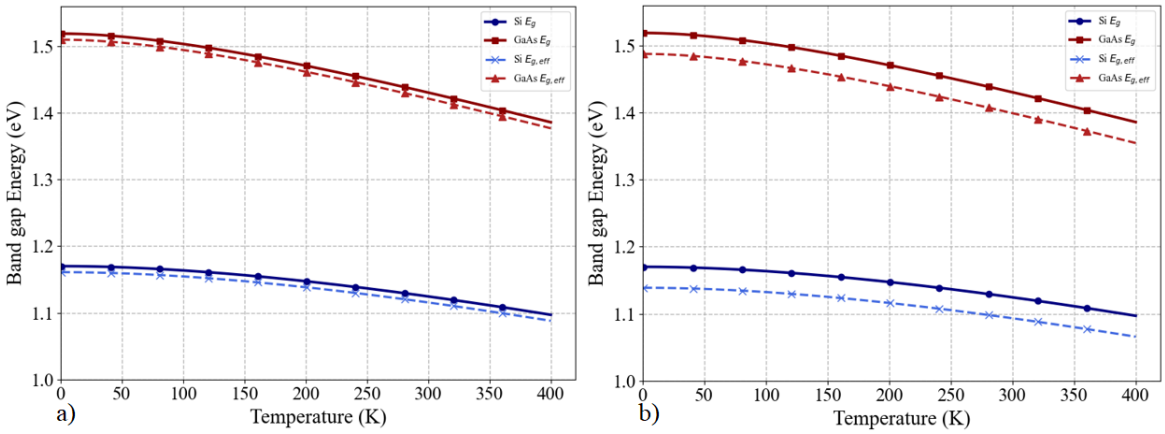

Figure 1. Fundamental and effective band gap energy versus temperature for Si and GaAs calculated using the Varshni relation and bandgap energy-narrowing (BGN) correction:(a) $N_d = N_a = 1\times10^{17}$ cm^{-3};(b) $N_d = N_a = 1\times10^{18}$ cm^{-3}.

Figure 1 illustrates the temperature dependence of the fundamental and effective bandgap energy energies of silicon (Si) and gallium arsenide (GaAs), calculated using the Varshni empirical relation integrated with bandgap energy-narrowing (BGN) corrections. The analysis considers doping concentrations of $N_d = N_a = 1\times10^{17}$ cm^{-3}[Fig. 1(a)] and 1×10^{18} cm^{-3}[Fig. 1(b)] over a wide temperature range from 4 K to 400 K.

The combined influence of temperature and doping on $E_g(T)$ and $E_{g,eff}(T)$ plays a decisive role in determining the optical and electronic performance of semiconductors. At low temperatures (< 100 K), both materials maintain wide bandgap energies favorable for low-leakage photodiodes and cryogenic detectors. In the intermediate range (200–300 K), the gradual reduction of $E_g(T)$ and $E_{g,eff}(T)$ strongly affects the intrinsic carrier concentration $n_i \propto \exp(-E_g/2kT)$, and thus the junction leakage currents in diodes and transistors. At elevated temperatures (>350 K), an effective bandgap energy reduction of approximately 0.05 eV in Si increases the intrinsic carrier concentration n_i by more than two orders

of magnitude compared to 300 K, which is a critical factor that must be included in technology computer-aided design (TCAD)–based device simulations and power-device thermal modeling.

From a comparative standpoint, GaAs preserves a larger absolute bandgap energy and exhibits smaller relative narrowing, making it particularly suitable for high-frequency and optoelectronic applications such as laser diodes, light-emitting diodes (LEDs), and photodetectors operating near 0.87 μm. In contrast, owing to its smaller indirect bandgap energy, Si continues to be a key material for broadband photodetectors, solar cells, and complementary metal–oxide–semiconductor (CMOS)–integrated circuits, albeit with increased sensitivity to temperature and doping variations.

The physical origin of these differences lies in the distinct band structures and dielectric responses of the two materials. Si exhibits stronger electron–phonon coupling and weaker dielectric screening ($\varepsilon \approx 11.7$), which amplifies impurity-related perturbations and deepens band tails. GaAs, characterized by a direct Γ-valley conduction band and higher dielectric constant ($\varepsilon \approx 13.1$), provides enhanced carrier screening and optical stability. Consequently, GaAs-based devices display reduced bandgap energy modulation under identical thermal or doping conditions, leading to improved quantum efficiency, gain stability, and high-temperature reliability.

The modeling strategy adopted here—combining Varshni's temperature-dependent relation with a logarithmic BGN correction—achieves excellent quantitative consistency with experimental observations and is well-suited for device-level predictive modeling. The inclusion of a 40 meV narrowing at $N = 10^{18}$ cm^{-3} alters the built-in potential (V_{bi}) and carrier lifetime predictions by 5–7 %, underscoring the importance of incorporating BGN effects into TCAD simulations of Si/GaAs heterojunctions, tandem solar cells, and LED/laser structures. Silicon-based devices: The stronger BGN effect in Si necessitates precise calibration of junction potential, carrier lifetime, and dark current in heavily doped regions. This is particularly critical for power electronic, photovoltaic, and CMOS applications, where carrier transport and leakage strongly depend on $E_{g,eff}(T)$. GaAs-based devices: The comparatively stable effective bandgap energy enhances optical confinement, carrier mobility, and thermal reliability, making GaAs superior for high-speed and high-temperature optoelectronic systems, including microwave photonics, laser diodes, and quantum well structures. Si/GaAs heterojunctions: Understanding the interplay of thermal and doping effects allows precise band alignment engineering, minimizing interface recombination and optimizing carrier extraction in multilayer and tandem architectures. Such insights are crucial for achieving high-efficiency heteroepitaxial photodiodes, tandem solar cells, and integrated optoelectronic circuits.

Future studies should extend this approach by incorporating strain-induced band modulation, quantum confinement, and alloy composition effects (e.g., GaAsP, InGaAs, or SiGe) to refine predictive accuracy for nanoscale and heteroepitaxial systems. These refinements are essential for the next generation of photonic, quantum, and energy-conversion devices, where accurate bandgap energy engineering governs both conversion efficiency and long-term operational stability. Integrating temperature, doping, strain, and compositional effects into unified analytical–computational frameworks will enable precise material tailoring, paving the way for high-efficiency, low-loss, and thermally robust semiconductor technologies.

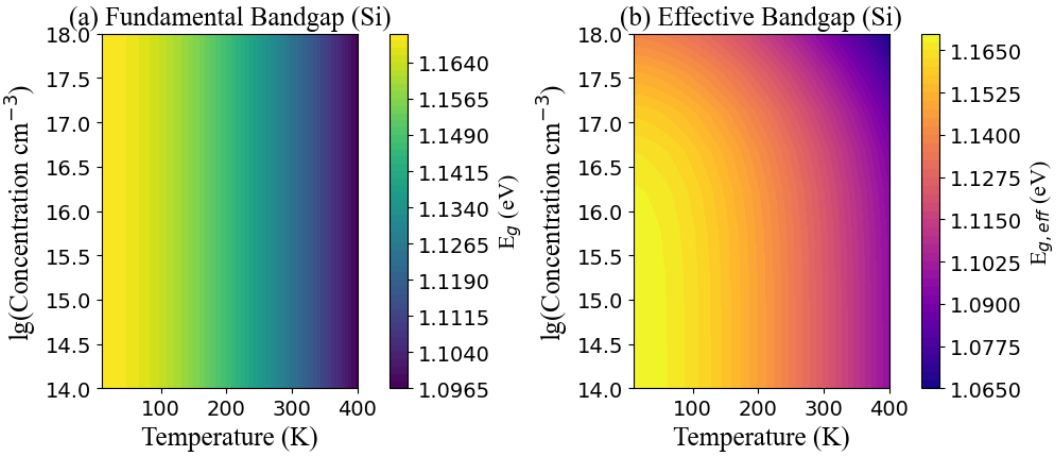

Figure 2. Temperature dependence of (a) the fundamental and (b) the effective band gap energy of Si.

Figures 2 and 3 depict the temperature-dependent evolution of the fundamental and effective band gap energies for silicon (Si) and gallium arsenide (GaAs), respectively, within the temperature range of 10–400 K and the doping concentration range of 10^{14}–10^{18} cm^{-3}. Both materials demonstrate a continuous reduction in band gap energy as the temperature increases, a behavior primarily governed by lattice thermal expansion and electron–phonon coupling effects as expressed by the Varshni relation. For silicon (Figure 2), the fundamental band gap $E_g(T)$ decreases from 1.170 eV at 0 K to approximately 1.103 eV at 400 K, resulting in an average thermal coefficient of $\frac{dE_g}{dT} \approx -1.7 \times 10^{-4}$ eV/K. This relatively weak temperature dependence arises from the large Varshni parameter $\beta_{Si} = 636$ K, indicating a modest phonon-induced band renormalization. When the bandgap energy narrowing (BGN) effect is included, the effective band

gap energy $E_{g,eff}(T)$ decreases further. At a moderate doping level of N = 10^{16} cm^{-3}, the bandgap energy reduction is approximately 0.01 eV, whereas at N = 10^{18} cm^{-3}, it reaches 0.06–0.07 eV. Consequently, $E_{g,\text{eff}}$for heavily doped Si falls to around 1.04 eV at 300 K, reflecting the impact of impurity-induced potential fluctuations and the merging of conduction and valence band tails.

In the case of GaAs (Figure 3), the fundamental band gap exhibits a more pronounced temperature sensitivity due to its smaller Varshni β parameter ($\beta_{\text{GaAs}} = 204$ K). The band gap decreases from 1.519 eV at 0 K to approximately 1.420 eV at 400 K, corresponding to a thermal coefficient of $\frac{dEg}{dT} \approx -2.5 \times 10^{-4}$ eV/K. This indicates that the electron–phonon interaction in GaAs is roughly 1.5 times stronger than in Si. When the doping-induced narrowing is included, the effective band gap $E_{g,eff}(T)$ drops to about 1.47 eV for N = 10^{16} cm^{-3} and further to 1.43 eV for N = 10^{18} cm^{-3}, implying a BGN magnitude of 40–50 meV at high doping levels. The weaker narrowing in GaAs compared to Si can be attributed to its direct band structure and lower density of states near the band edges, which reduces impurity band overlap.

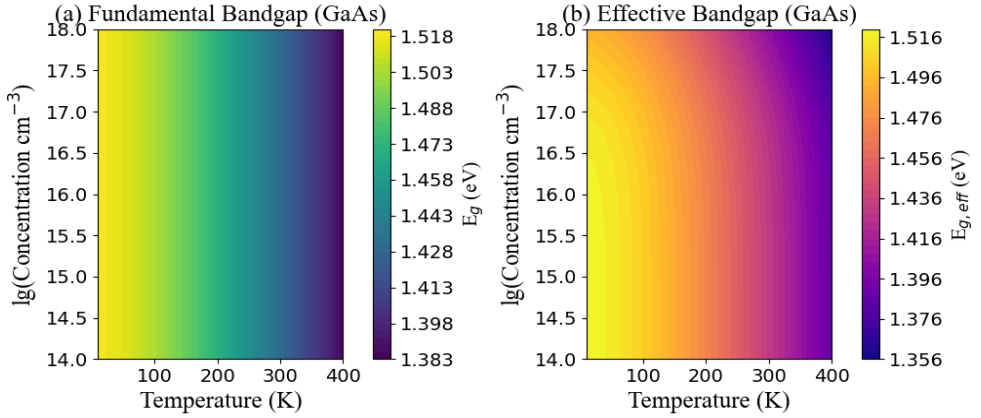

Figure 3. Temperature dependence of (a) the fundamental and (b) the effective band gap energy of GaAs.

A direct comparison between Figures 2 and 3 reveals several key differences. First, GaAs maintains a larger band gap across the entire temperature range by approximately 0.32–0.35 eV at 300 K making it more suitable for high-frequency and optoelectronic applications where direct interband transitions are desired. Second, the temperature coefficient of GaAs is nearly 50% larger than that of Si, indicating higher thermal sensitivity, which may limit its use in devices operating under elevated temperatures without compensation mechanisms. Third, Si exhibits stronger doping dependence, with an effective bandgap energy reduction exceeding 60 meV at $N = 10^{18}$ cm^{-3}, compared to 40–50 meV for GaAs under similar conditions. Overall, the comparative analysis indicates that Si is thermally more stable but more susceptible to impurity-induced band tailing, while GaAs offers superior optical properties but exhibits stronger temperature-induced bandgap energy reduction. These results are consistent with experimental observations and underline the necessity of temperature- and doping-dependent modeling in the design of Si- and GaAs-based optoelectronic and high-power devices.

Table 2. Comparison of intrinsic and effective intrinsic carrier concentrations in Si and GaAs at 300 K

Doping level (cm^{-3})	**ΔE$_{(BGN)}$ Si: (eV)**	**Si: n$_i$ (cm^{-3})**	**Si: n$_{i,}$eff (cm^{-3})**	**ΔE$_{(BGN)}$ GaAs: (eV)**	**GaAs: n$_i$ (cm^{-3})**	**GaAs: n$_{i,}$eff (cm^{-3})**
1×10^{14}	3.0×10^{-4}	1.50×10^{10}	1.51×10^{10}	1.1×10^{-5}	1.90×10^{6}	1.90×10^{6}
1×10^{15}	1.0×10^{-3}	1.50×10^{10}	1.53×10^{10}	1.1×10^{-4}	1.90×10^{6}	1.90×10^{6}
1×10^{16}	1.0×10^{-2}	1.50×10^{10}	1.82×10^{10}	1.03×10^{-3}	1.90×10^{6}	1.94×10^{6}
1×10^{18}	6.0×10^{-2}	1.50×10^{10}	4.79×10^{10}	2.60×10^{-2}	1.90×10^{6}	3.14×10^{6}
1×10^{19}	1.0×10^{-1}	1.50×10^{10}	1.04×10^{11}	5.01×10^{-2}	1.90×10^{6}	5.00×10^{6}

At 300 K, silicon (Si) and gallium arsenide (GaAs) demonstrate distinctly different doping responses in both their intrinsic and effective intrinsic carrier concentrations due to varying degrees of bandgap energy narrowing (BGN). As summarized in Table 2, the intrinsic carrier density of Si $n_i = 1.5 \cdot 10^{10}\ cm^{-3}$ is approximately four orders of magnitude higher than that of GaAs $1.9 \cdot 10^{6}\ cm^{-3}$, primarily due to Si's smaller bandgap energy. When the doping concentration rises from $1 \cdot 10^{14}\ cm^{-3}$ to $5 \cdot 10^{19}\ cm^{-3}$, Si exhibits a nearly sevenfold increase in its effective intrinsic concentration from $1.51 \cdot 10^{10}\ cm^{-3}$ to $1.04 \cdot 10^{11}\ cm^{-3}$ driven by a substantial bandgap energy reduction of $\Delta E_{BGN} \approx 0.01\ eV$. In contrast, GaAs experiences only a 2.6-fold enhancement $1.9 \cdot 10^{6}\ cm^{-3}$ to $5.0 \cdot 10^{6}\ cm^{-3}$ with a smaller $\Delta E_{BGN} \approx 0.05\ eV$. This sharp contrast highlights that Si is significantly more sensitive to heavy doping, leading to stronger bandgap energy narrowing and higher carrier activation, while GaAs maintains superior electronic stability with limited BGN effects an essential advantage for high-speed and high-temperature optoelectronic devices.

CONCLUSIONS

A comprehensive comparison of the intrinsic and effective intrinsic carrier concentrations and bandgap energy-narrowing (BGN) effects in Si and GaAs has been carried out at 300 K over doping levels ranging from 1×10^{14} to 1×10^{19} cm^{-3}. The results reveal that silicon (Si) exhibits a pronounced narrowing of the bandgap energy from 1.12 eV (intrinsic) to 1.02 eV at $N = 1\times10^{19}$ cm^{-3}, corresponding to $\Delta E_{BGN} \approx 0.10$ eV. In contrast, gallium arsenide (GaAs) shows a smaller reduction from 1.424 eV to 1.374 eV ($\Delta E_{BGN} \approx 0.05$ eV) under the same doping conditions. The effective intrinsic carrier concentration in Si rises sharply from 1.5×10^{10} cm^{-3} (intrinsic) to 1.0×10^{11} cm^{-3} at $N = 1\times10^{19}$ cm^{-3}—a nearly sevenfold enhancement. In GaAs, the corresponding increase is more moderate from 1.9×10^{6} cm^{-3} to 5.0×10^{6} cm^{-3} (a 2.6× growth). At moderate doping ($N = 1\times10^{16}$ cm^{-3}), Si experiences $\Delta E_{(BGN)} \approx 1.0\times10^{-2}$ eV and $n_{i,eff} \approx 1.8\times10^{10}$ cm^{-3}, whereas GaAs shows $\Delta E_{(BGN)} \approx 1.0\times10^{-3}$ eV and $n_{i,eff} \approx 1.9\times10^{6}$ cm^{-3} demonstrating nearly an order of magnitude weaker dependence on impurity concentration. This disparity originates from Si's higher effective density of states ($Nc \approx 2.8\times10^{19}$ cm^{-3}, $Nv \approx 1.04\times10^{19}$ cm^{-3}) and its indirect band structure, which enhances carrier–carrier and impurity interactions. GaAs, with $Nc \approx 4.7\times10^{17}$ cm^{-3} and $Nv \approx 7.0\times10^{18}$ cm^{-3}, exhibits stronger dielectric screening and less BGN sensitivity. At cryogenic conditions ($T < 20$ K), incomplete ionization becomes dominant: in Si, up to 80% of donors and acceptors remain un-ionized, reducing free-carrier density by nearly one order of magnitude; in GaAs, the ionization efficiency exceeds 90% under similar doping, maintaining higher conductivity stability. Consequently, Si is advantageous for cryogenic or high-field devices such as low-noise detectors and power diodes, whereas GaAs remains superior for high-frequency optoelectronic and microwave components. These quantitative insights into $\Delta E_{(BGN)}$ and $n_{i,eff}$ provide a reliable framework for predictive bandgap energy engineering and doping optimization in next-generation Si-, GaAs-, and Si/GaAs-based heterostructures and nanodevices.

ORCID

Jonibek Sh. Abdullayev, https://orcid.org/0000-0001-8950-2135
Madinabonu Sh. Ibragimova, https://orcid.org/0009-0004-7867-7086
Jo'shqin Sh. Abdullayev, https://orcid.org/0000-0001-6110-6616
Ibrokhim B. Sapaev, https://orcid.org/0000-0003-2365-1554

REFERENCES

[1] A. Qu, Z. Xie, Y. Wang, *et al.* "Effect of Acceptor-Type Traps in GaN Buffer Layer on Current Collapse of ε-Ga_2O_3/GaN HEMTs," J. Electron. Mater. **54**, 3086–3096 (2025). https://doi.org/10.1007/s11664-025-11823-9

[2] J.S. Abdullayev, D.A. Qalandarova, M.S. Ibragimova, *et al*. "Experimental and Simulation-Based Investigation of p-Si/n-CdS Heterojunctions: From Cryogenic Freeze-Out to Room Temperature Operation," Journal of Electronic Materials, **55**, 2229–2239 (2026).https://doi.org/10.1007/s11664-025-12642-8

[3] B. Abdullaev, and D. Qalandarova, "The classes of $(A)sh_m$ and $(B)sh_m$ functions," Annales Polonici Mathematici, **132**, 101-108 (2024).https://doi.org/10.4064/ap230727-30-11

[4] G.S. Sahoo, C. Harini, N. Mahadevi, P.S. Nethra, A. Tripathy, M. Verma, and G.P. Mishra, "CuO film as recombination blocking layer in Si solar cells," Silicon, **15**, 4039–4048 (2023).https://doi.org/10.1007/s12633-023-02701-x

[5] I.B. Sapaev, J.I. Razzokov, J.S. Abdullayev, D.A. Qalandarova, and M.S. Ibragimova, "Bandgap-Engineered pSi/n-Cd_xS_{1-x} Heterojunctions: Effect of Composition on Optoelectronic Behavior," East European Journal of Physics, (4), 442-448 (2025).https://doi.org/10.26565/2312-4334-2025-4-44

[6] S. Fan, Z.J. Yu, Y. Sun, W. Weigand, P. Dhingra, M. Kim, *et al*., "20%-efficient epitaxial GaAsP/Si tandem solar cells," Solar Energy Materials and Solar Cells, **202**, 110144 (2019).https://doi.org/10.1016/j.solmat.2019.110144

[7] J.Sh. Abdullayev, I.B. Sapaev, J.Sh. Abdullayev, D. A. Juraev, M. J. Jalalov, E. E. Elsayed, "Mathematical modeling of incomplete ionization in radial p-Si/n-GaAs heterojunctions: temperature and doping effects", Journal of Electronic Materials, **54**, 1–9 (2025).https://doi.org/10.1007/s11664-025-12391-8

[8] D. Li, C. Luo, H. Wang, F. Ling, and J. Yao, "Active control of plasmon-induced transparency based on a GaAs/Si heterojunction in the terahertz range," Optical Materials, **114**, 111609 (2021).https://doi.org/10.1016/j.optmat.2021.111609

[9] M.N. Hasan, Y. Zheng, J. Lai, E. Swinnich, O.G. Licata, M.A. Baboli, B. Mazumder, *et al*., "Influences of native oxide on the properties of ultrathin Al_2O_3-interfaced Si/GaAs heterojunctions," Advanced Materials Interfaces, **9**(13), 2101531 (2022). https://doi.org/10.1002/admi.202101531

[10] J.Sh. Abdullayev, and I.B. Sapaev, "Optimizing the influence of doping and temperature on the electrophysical features of p-n and p-i-n junction structures," Eurasian Physical Technical Journal, **21**(3(49)), 21-28 (2024). https://doi.org/10.31489/2024No3/21-28

[11] M. Jurisch, F. Börner, T. Bünger, S. Eichler, T. Flade, U. Kretzer, A. Köhler, *et al*., "LEC- and VGF-growth of SI GaAs single crystals – Recent developments and current issues," Journal of Crystal Growth, **275**(1–2), 283–291 (2005).. https://doi.org/10.1016/j.jcrysgro.2004.10.092

[12] R.S. Singh, R.D. Patidar, K. Deshmukh, *et al.* "Influence of CuO Layer on the Performance of Thin-Film Copper Indium Gallium Selenide Solar Cells: A Numerical Analysis," J. Electron. Mater. **54**, 609–619 (2025). https://doi.org/10.1007/s11664-024-11588-7

[13] J.Sh. Abdullayev, and I.B. Sapaev, "Factors influencing the ideality factor of semiconductor p-n and p-i-n junction structures at cryogenic temperatures," East European Journal of Physics, (4), 329–333 (2024). https://doi.org/10.26565/2312-4334-2024-4-37

[14] T. Chen, G. Wu, H. Qiao, *et al.* "Si@perovskite nanowire design by Si scattering to enhance perovskite optical response," Opt Quant Electron, **57**, 333 (2025). https://doi.org/10.1007/s11082-025-08258-1

[15] J. Herfort, H.-P. Schönherr, and K.H. Ploog, "Epitaxial growth of hybrid structures," Applied Physics Letters, **83**(18), 3912–3914 (2003). https://doi.org/10.1063/1.1625426

[16] J.Sh. Abdullayev, and I.B. Sapaev, "Modeling and calibration of electrical features of p-n junctions based on Si and GaAs," Physical Sciences and Technology, **11**(3–4), 39–48 (2024). https://doi.org/10.26577/phst2024v11i2b05
[17] J.Sh. Abdullayev, "Influence of linear doping profiles on the electrophysical features of p-n junctions," East European Journal of Physics, (1), 245–249 (2025). https://doi.org/10.26565/2312-4334-2025-1-26
[18] E.P. Devine, T. Yamada, S.Y. Wang, *et al.* "Stacked co-packaged Si-Ge-Si photodetectors with > 60 GHz bandwidth for near-infrared wavelength-simulation," Discov Electron, **2**, 99 (2025). https://doi.org/10.1007/s44291-025-00137-z
[19] A.B. Roy, N.H.R. Valiji, R. Mohammad, P. Giridhar, and P. Mondal, "Performance enhancement of Si/GaAs based heterojunction solar cells by opto-electronics modeling and optimization," in: *2024 International Conference on Recent Advances in Electrical, Electronics, Ubiquitous Communication, and Computational Intelligence (RAEEUCCI*), (IEEE, 2024), pp. 1–6. https://doi.org/10.1109/RAEEUCCI61380.2024.10547792
[20] K.K.D. Nigam, P. Yadav, *et al.*, "Numerical Investigation of $RbGeI_3$-Based Lead-Free Perovskite Solar Cell with Various Cu-Based Hole Transport Layers Using SCAPS-1D," J. Electron. Mater. **54**, 2747–2765 (2025). https://doi.org/10.1007/s11664-025-11740-x
[21] J.Sh. Abdullayev, and I.B. Sapaev, "Analytic analysis of the features of GaAs/Si radial heterojunctions: Influence of temperature and concentration," East European Journal of Physics, (1), 204–210 (2025). https://doi.org/10.26565/2312-4334-2025-1-21
[22] M. Piriyev, G. Loget, Y. Léger, L. Chen, A. Létoublon, T. Rohel, C. Levallois, *et al*., "Dual bandgap energy operation of a GaAs/Si photoelectrode," Solar Energy Materials and Solar Cells, **251**, 112138 (2023). https://doi.org/10.1016/j.solmat.2022.112138
[23] J.Sh. Abdullayev, I.B. Sapaev, N. Esanmuradova, S. Kadirov, and S. Kuliyev, "Mathematical analysis of the features of radial p-n junction: Influence of temperature and concentration," East European Journal of Physics, (2), 220–225 (2025). https://doi.org/10.26565/2312-4334-2025-2-24
[24] J. Alanis, S.J. Gutiérrez-Ojeda, R. Méndez-Camacho, and E. Cruz-Hernández, "Theoretical investigation of the growth of GaAs on Si(001), Si(110), Si(111), Si(113), and Si(331)," Surfaces and Interfaces, **44**, 103792 (2024). https://doi.org/10.1016/j.surfin.2023.103792
[25] J.Sh. Abdullayev, and G.Kh. Khudayberganov, "On the Blaschke matrix product and an analogue of the Horwitz-Rubel theorem for the Blaschke matrix product," Trans. Natl. Acad. Sci. Azerb. Ser. Phys.-Tech. Math. Sci. Mathematics, **45**(4), 3-19 (2025). https://doi.org/10.30546/2617-7900.45.4.2025.019
[26] R. Huang, Q. Wang, Y. Guo, and Z. Wang, "Comparative study on GaAs/Si heterojunction fabricated by nitrogen and oxygen plasma activated bonding," Vacuum, **208**, 111735 (2023). https://doi.org/10.1016/j.vacuum.2022.111735
[27] J. Kaarthik, S. Biswas, N. Ram, *et al*. "Thickness-Dependent Resistive Switching Characteristics in $HfO_2/SiO_2/Si$ Memristive Devices," J. Electron. Mater. **54**, 7731–7739 (2025). https://doi.org/10.1007/s11664-025-12134-9
[28] J. Liang, L. Chai, S. Nishida, M. Morimoto, and N. Shigekawa, "Investigation on the interface resistance of Si/GaAs heterojunctions fabricated by surface-activated bonding," Japanese Journal of Applied Physics, **54**(3), 030211 (2015). https://doi.org/10.7567/JJAP.54.030211
[29] M. Haris, S.A. Loan, and Mainuddin," "Si/GaAs hetero junction tunnel FET: Design and investigation," Journal of Nanoelectronics and Optoelectronics, **14**(10), 1434–1444 (2019). https://doi.org/10.1166/jno.2019.2575
[30] J. Liang, T. Miyazaki, M. Morimoto, S. Nishida, N. Watanabe, and N. Shigekawa, "Electrical properties of p-Si/n-GaAs heterojunctions by using surface-activated bonding," Applied Physics Express, **6**(2), 021801 (2013). https://doi.org/10.7567/APEX.6.021801
[31] E. Widianto, M. Riswan, C. Driyo, *et al*. "Interfacial Engineering Using Low-Temperature Indium Sulfide Electron-Transporting Material for Efficient Sn-Based Perovskite Solar Cells," J. Electron. Mater. **53**, 7642–7654 (2024). https://doi.org/10.1007/s11664-024-11488-w
[32] P.B. Mittal, "Core–Shell Incorporated Analytical Modeling of a Dual-Material Gate Junctionless Nanowire: Extraction of Subthreshold Characteristics," J. Electron. Mater. **54**, 3046–3059 (2025). https://doi.org/10.1007/s11664-025-11737-6
[33] O. Tukfatullin, B. Butunbaev, and S. Otaboev, Front-Surface Soiling Measurement Device for Photovoltaic Modules. Vidnovluvana Energetyka, **4**(83), 189-194 (2025). https://doi.org/10.36296/1819-8058.2025.4(83).189-194
[34] N. Moussaoui, L. Benhamadouche, and A.D. Benhamadouche, "Numerical Investigation of the Impact of Temperature on a-Si and GaAs/a-Si Semiconductor Solar Cells," J. Electron. Mater. **53**, 6803–6810 (2024). https://doi.org/10.1007/s11664-024-11364-7
[35] T. Yu, H. Zhang, D. Li, and Y. Lu, "Electronic and optical properties of silicene on GaAs(111) with hydrogen intercalation: A first-principles study," RSC Advances, **11**, 16040–16050 (2021). https://doi.org/10.1039/D1RA01959G
[36] R.A. Muminov, V.G. Dyskin, O.F. Tukfatullin, *et al*., "Study of the Effect of Optical Constants of Dust Film on the Efficiency of Photovoltaic Modules," Appl. Sol. Energy, **60**, 829–834 (2024). https://doi.org/10.3103/S0003701X25600766
[37] R. Huang, Z. Wang, K. Wu, H. Xu, Q. Wang, and Y. Guo, "Hybrid bonding of GaAs and Si wafers at low temperature by Ar plasma activation," Journal of Semiconductors, **45**(4), 042701 (2024). https://doi.org/10.1088/1674-4926/45/4/042701
[38] A.A. Sushkov, D.A. Pavlov, A.I. Andrianov, V.G. Shengurov, S.A. Denisov, V.Y. Chalkov, R.N. Kriukov, *et al*., "Comparison of III–V heterostructures grown on Ge/Si, Ge/SOI, and GaAs," Semiconductors, **56**, 122–133 (2022). https://doi.org/10.1134/S106378262201012X
[39] P.K. Saxena, P. Srivastava, and A. Srivastava, "Defect analysis of MBE reactor-grown HgCdTe on Si, GaAs, GaSb, and CZT substrates through the TNL-Epigrow simulator," Journal of Electronic Materials, **53**, 5803–5812 (2024). https://doi.org/10.1007/s11664-024-11082-0
[40] U.S. Rakhmonov, and J.Sh. Abdullayev, "On properties of the second type matrix ball $B_{m,n}^2$ from space C[m×n]", J. Sib. Fed. Univ. Math. Phys. **15**(3), 329–342 (2022).
[41] M. Kria, M. El-Yadri, L.M. Pérez, E. Feddi, *et al*., "Thermodynamic and magnetic properties of cylindrical nanoshell GaAsMn considering Rashba spin–orbit coupling," Physica Scripta, **100**(8), (2025). https://doi.org/10.1088/1402-4896/adf57c
[42] D.Q. Fang, A.L. Rosa, Th. Frauenheim, and R.Q. Zhang, "Band gap engineering of GaN nanowires by surface functionalization," Applied Physics Letters, **94**(7), 073116 (2009). https://doi.org/10.1063/1.3086316
[43] A. Rejmer, A. Ozcan-Atar, W. Kołkowski, I. Pasternak, S. Kozdra, A. Materna, E. Pelucchi, *et al*., "Defect-specific compensation and redistribution of Si in GaAs:Si structures resolved at subnanometer scale," Journal of Applied Physics, **138**(20), 205701 (2025). https://doi.org/10.1063/5.0281923

КРІОГЕННІ МАТЕРІАЛЬНІ ТА ЕЛЕКТРОФІЗИЧНІ ЗМІНИ В Si ТА GaAs

Джонібек Ш. Абдуллаєв[1], Мадінабону Ш. Ібрагімова[1], Джошкін Ш. Абдуллаєв[2], Іброхім Б. Сапаєв[2,3,4,5]

[1]Ургенчський державний університет, вулиця Хаміда Олімджона, 14, Ургенч, 220100 Узбекистан

[2]Національний дослідницький університет ТІІАМ, кафедра фізики та хімії, Ташкент, Узбекистан

[3]Західно-Каспійський університет, Баку, Азербайджан

[4]Ташкентський університет прикладних наук, вулиця Університетська, 28, Ташкент 100095, Узбекистан

[5]Інженерний факультет, Центральноазіатський університет, Ташкент 111221, Узбекистан

У цьому дослідженні систематично вивчено кріогенну поведінку кремнію (Si) та арсеніду галію (GaAs) у температурному діапазоні 4–300 K та при концентраціях легування від власних до 1×10^{18} $см^{-3}$. Встановлено еволюцію фундаментальної та ефективної ширини забороненої зони: у Si вона зростає від 1,12 до 1,17 еВ, а у GaAs — від 1,42 до 1,51 еВ при зниженні температури від 300 K до 4 K. Визначено енергії активації донорів і акцепторів, які демонструють виражений ефект неповної іонізації при $T < 20$ K, що зменшує концентрацію вільних носіїв майже на 80% у слабко легованих зразках і суттєво знижує електропровідність. Аналіз поверхневої хімічної стабільності показав придушення дифузії легуючих домішок та мінімальну окиснюваність у кріогенних умовах. Отримані результати забезпечують комплексне розуміння взаємодії структурних, електронних та хімічних процесів у Si і GaAs, що є критично важливим для проєктування та оптимізації кріогенних електронних і оптоелектронних пристроїв.

Ключові слова: *ефективна ширина забороненої зони; електростатичний потенціал; неповна іонізація; концентрація носіїв; розширення забороненої зони; ефекти низьких температур; кріогенні напівпровідники; електропровідність*